Title
Hyperbolic metamaterial as super absorber for scattered fields generated at its surface

Journal
Physical Review B, 86(20)

ISSN
2469-9950

Authors
Guclu, Caner
Campione, Salvatore
Capolino, Filippo

Publication Date
2012-11-15

DOI
10.1103/physrevb.86.205130

Hyperbolic metamaterial as super absorber for scattered fields generated at its surface

Caner Guclu, Salvatore Campione, and Filippo Capolino*

Department of Electrical Engineering and Computer Science, University of California, Irvine, CA 92697, USA

(Received 16 July 2012; revised manuscript received 1 November 2012; published 29 November 2012)

We show that hyperbolic metamaterials (HMs) that exhibit hyperbolic wave-vector dispersion diagrams possess two important features related to super absorption: The total power scattered by a nanosphere is (i) greatly enhanced when placed at the HM surface, compared to other material surfaces, and (ii) almost totally directed into the HM. We show that these two features are peculiar of HM interfaces, and we support them using a spectral theory study of transverse-electric and magnetic waves scattered by a subwavelength nanosphere. We analyze the nanosphere's scattered power absorbed by various substrate configurations. We also consider various nanosphere materials.

DOI: 10.1103/PhysRevB.86.205130 PACS number(s): 42.25.Fx, 78.20.Ci, 72.80.Tm, 78.67.Pt

I. INTRODUCTION

Composite hyperbolic metamaterials (HMs) are a particular kind of uniaxial anisotropic materials with an isofrequency hyperbolic-like wave-vector dispersion diagram[1,2] (as stated in Sec. II, the wave-vector dispersion curve of a realistic HM is not an exact hyperbola).

The aim of this paper is to use a spatial spectrum approach[1] to show that a HM may exhibit the potential to act as a super absorber for scattered fields generated by a nanoparticle near its surface. In other words, two important phenomena occur: (i) The nanoparticle's scattered fields will be enhanced by the presence of the HM, and (ii) fields are mainly directed into the HM, and hence are almost totally absorbed there. Implicitly, this means that the local density of states, related to the total emitted power of a dipole, is greatly increased. These physical properties are of key importance and allow us to foresee broadband wide-angle absorption when scattering is created at the HM surface, by either purposely roughening a HM surface or, equivalently, locating many nanoscatterers at the HM surface.

The use of spectral theory enables us to carefully analyze the radiation capabilities of elementary dipoles or small objects located close to HMs for different physical conditions including, but not limited to, distance from the HM, materials, shapes, and source power spectra. In particular, we analyze systematically all the physical parameters that affect absorption capabilities, and we quantify their effect. This work aims at providing a clear and exhaustive analysis of the interaction between a single dipole, or a nanoscatterer, and a HM. This analysis may lead to possible developments of innovative ways to absorb fields at microwaves as well as millimeter-wave, infrared, and optical frequencies, since HM fabrication using composite materials is simple and does not require extreme, unfeasible material parameters. The HM considered here is either made by a multilayered metal–dielectric composite or is a homogeneous HM. In both cases, we demonstrate the HM suitability to super absorption capabilities, which are consistent also with other HM implementations as well (e.g., wire medium). We show that when a homogeneous HM is considered, the absorption properties discussed in this paper are slightly overestimated when compared to a multilayered HM implementation. The formulation shown here is general and can be applied to other envisioned applications involving HMs, not limited to absorption properties. Note that the design of a practical absorber would require the analysis of many nanoscatterers in proximity of the HM, and as such we postpone this discussion to a future effort.

Multilayered structures as in Fig. 1 are practical implementations of HMs at optical frequencies and have been investigated for negative refraction,[3] subwavelength field focusing, and superlensing applications.[4–10] The spontaneous emission patterns of electric and magnetic dipoles above a multilayer HM surface were estimated using the dyadic Green's function technique in Ref. 11. An increased rate of spontaneous emission near nanostructured HMs has been reported in Ref. 12. The absorption of thin dye-doped polymeric films located on top of several substrates (glass, silver, gold, and multilayered HMs) has been shown in Ref. 13, concluding that absorption can be tuned and enhanced by controlling the substrate geometry and composition. As a result of a recent experiment in Ref. 14, corrugated surfaces of HMs lead to a very low reflectance and ultimate dark appearance, providing a further incentive to the analysis here proposed.

The outline of the paper is as follows. We first model multilayered HMs in Sec. II using both effective medium approximation (EMA) and Bloch theory, showing that the former is applicable under certain limitations and in general overestimates results for the multilayered systems. Then we study in Sec. III the power emitted by an impressed dipole close to HMs via spectral theory. We then extend in Sec. IV the developed theory to analyze the power scattered by a nanoparticle close to HMs. Conclusions and final remarks are stated in Sec. V.

II. LAYERED HYPERBOLIC METAMATERIAL AND LIMITATION OF EFFECTIVE MEDIUM APPROXIMATION

Consider a structure made by a stack of two homogeneous layers as in Fig. 1, with subwavelength thicknesses d_1 and d_2, and with relative permittivities $\varepsilon_1 = \varepsilon_1' + i\varepsilon_1''$ and $\varepsilon_2 = \varepsilon_2' + i\varepsilon_2''$ (a prime and a double prime denote real and imaginary parts, respectively). This multilayered structure can be approximated by a homogeneous HM via EMA having the anisotropy axis coincident with the z axis and permittivity tensor

$$\underline{\varepsilon}_{\mathrm{HM}} = \varepsilon_t(\hat{\mathbf{x}}\hat{\mathbf{x}} + \hat{\mathbf{y}}\hat{\mathbf{y}}) + \varepsilon_z\hat{\mathbf{z}}\hat{\mathbf{z}}, \tag{1}$$

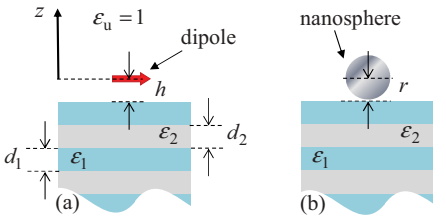

FIG. 1. (Color online) (a) Elementary dipole at a distance h from the interface between free space (upper space, denoted with subscript u) and a multilayered HM. (b) A nanosphere with radius r, located at the HM surface.

where the expressions for $\varepsilon_t = \varepsilon_t' + i\varepsilon_t''$ and $\varepsilon_z = \varepsilon_z' + i\varepsilon_z''$ are[15]

$$\varepsilon_t = \frac{\varepsilon_1 d_1 + \varepsilon_2 d_2}{d_1 + d_2} \quad \varepsilon_z^{-1} = \frac{\varepsilon_1^{-1} d_1 + \varepsilon_2^{-1} d_2}{d_1 + d_2}. \tag{2}$$

Assume for the moment absence of material losses (i.e., $\varepsilon'' = 0$): A HM can be easily realized by choosing $\varepsilon_1 < 0$ (metallic layer at optical frequencies) and $\varepsilon_2 > 0$ (dielectric layer). In general, two categories of plane waves, namely, ordinary and extraordinary waves, are present in a uniaxial anisotropic medium propagating with $\exp[i(k_x x + k_y y + k_z z)]$, as described in Ref. 16, where k_z and $k_t = (k_x^2 + k_y^2)^{1/2}$ are the z and the *transverse to z* components of the wave vector $\mathbf{k} = k_x\hat{\mathbf{x}} + k_y\hat{\mathbf{y}} + k_z\hat{\mathbf{z}}$. As shown already in Ref. 16, when considering a homogeneous HM with uniaxial anisotropy of permittivity, ordinary waves are TE (E field transverse to z) and related to ε_t. Similarly, extraordinary waves are TM (H field transverse to z) and exhibit a hyperbolic wavevector dispersion when $\varepsilon_t \varepsilon_z < 0$.[16] The dispersion relations of ordinary and extraordinary waves are given by

$$\begin{aligned} \text{TE (ordinary):} \quad & \frac{k_t^2 + k_z^2}{\varepsilon_t} = k_0^2, \\ \text{TM (extraordinary):} \quad & \frac{k_t^2}{\varepsilon_z} + \frac{k_z^2}{\varepsilon_t} = k_0^2, \end{aligned} \tag{3}$$

where k_0 is the wave number in free space. In principle, the case with $\varepsilon_z < 0$, $\varepsilon_t > 0$ allows the extraordinary waves to propagate (carry power) in the HM for any k_t, whereas the ordinary waves propagate only for $k_t < k_0\sqrt{\varepsilon_t}$, provided EMA holds (see the discussion regarding Fig. 3). When $\varepsilon_z > 0$, $\varepsilon_t < 0$, instead, extraordinary waves propagate in the HM for any $k_t > k_0\sqrt{\varepsilon_z}$, whereas ordinary waves are evanescent in the whole spectrum, provided EMA holds. This latter HM case is investigated here because its realistic design is achievable over a wide bandwidth at optical frequencies when using metallic (with large negative relative permittivity values) and dielectric layers. It is fundamental to observe that TM waves can propagate in the HM up to very large values of k_t that would otherwise be evanescent in the upper isotropic half-space, resulting in the energy transfer from the evanescent spectrum in free space into a propagating one in the HM.

Consider now a lossy multilayered HM shown in Fig. 1 made of $d_1 = d_2 =$ 5-nm-thick silver (complex permittivity obtained from Ref. 17) and silica ($\varepsilon_{SiO_2} = 2.2$) layers. This leads to the permittivity tensor entries ε_t and ε_z evaluated by EMA shown in Fig. 2 with $\varepsilon_t' < 0$ and $\varepsilon_z' > 0$ for the

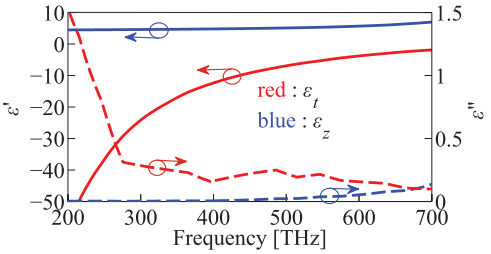

FIG. 2. (Color online) Effective $\varepsilon_t = \varepsilon_t' + i\varepsilon_t''$ and $\varepsilon_z = \varepsilon_z' + i\varepsilon_z''$ evaluated by EMA versus frequency, pertaining to the HM made of silica ($\varepsilon_{SiO_2} = 2.2$) and silver layers, with thicknesses $d_1 = d_2 = 5$ nm.

entire frequency band analyzed here, thus imposing hyperbolic dispersion diagrams. It has been recently reported in Ref. 18 that the power directed toward the metal–dielectric multilayers is overestimated by EMA, and we provide here a discussion on the reasons behind this phenomenon. We employ Bloch theory[19] to determine the dispersion diagram complex k_z versus real k_t (with $k_z = \beta_z + i\alpha_z$) for TM waves inside the HM at 400 THz, reported in Fig. 3 (solid blue curve) and compared to the dispersion diagram obtained by EMA (dashed red curve). In Fig. 3, we only show the mode with $\beta_z > 0$ and $\alpha_z < 0$, because it is the only one decaying (carrying power) in the $-z$ direction, inside the HM. The curve shows that the wave propagating inside the HM is backward because $\beta_z \alpha_z < 0$.[20,21] The $-k_z$ solution, with $\beta_z < 0$ and $\alpha_z > 0$, would be the equivalent solution decaying in the $+z$ direction. We note that similar diagrams are preserved at other frequencies as well (see the discussion in Sec. III and Fig. 6).We observe that for a wide k_t spectrum, the real part of the wave number β_z computed by Bloch theory is close to the hyperbola obtained by EMA, confirming a hyperbolic-like dispersion (Fig. 3). However, for larger k_t, the dispersion curve significantly deviates from the one obtained by EMA, and it is not hyperbolic anymore. Indeed, close to $k_t \approx 14.3k_0$, β_z approaches the Brillouin zone

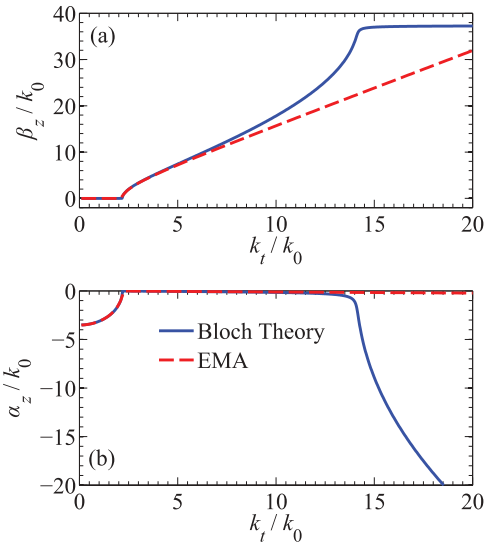

FIG. 3. (Color online) $k_z - k_t$ dispersion diagram normalized by k_0. (a) Real and (b) imaginary parts of the wave number $k_z = \beta_z + i\alpha_z$ in the multilayered HM with periodicity $d = d_1 + d_2 = 10$ nm $\approx \lambda_0/75$ at 400 THz obtained via Bloch theory and EMA.

edge ($\beta_z \approx 37.5k_0 \approx \pi/d$ at 400 THz, where $d = d_1 + d_2$ is the period), and thereafter the attenuation constant α_z increases dramatically (behavior not modeled by EMA), marking a mainly evanescent spectrum in the HM. It is observed that even for small constituent-layer thicknesses and for large k_t it is important to take into account the heterogeneity of layered structures because a large wave number k_z implies a short wavelength in the z direction. Hence, a maximum propagating k_t spectral limit can be determined. Therefore, one should not rely on EMA for large wave numbers because EMA does not introduce any limitation for the propagating spectrum, i.e., theoretically all $k_t \in (k_{t,\,\mathrm{min}}, \infty)$ would propagate in the HM, where $k_{t,\,\mathrm{min}}$ is determined following the discussion after Eq. (3). In other words, according to EMA, the emitted power spectrum coupled to the HM is limited only by the spatial spectrum of the field at the HM interface, and therefore EMA could lead to overestimation of the power emitted by physically very small sources (characterized by a very wide spatial spectrum of emission). It is for these reasons that in the following, we mainly treat the HM as a nonhomogeneous medium modeled via Bloch theory, and we also provide results regarding the HM modeled by EMA in order to determine its validity range.

III. SPECTRAL THEORY AND POWER EMITTED BY AN IMPRESSED DIPOLE CLOSE TO A HYPERBOLIC METAMATERIAL

We consider first the power emitted by a transverse elementary dipole with electric polarization $\mathbf{P} = p_x \hat{\mathbf{x}} \delta(\mathbf{r})$ located close to the interface between free space and the HM as illustrated in Fig. 1(a). To gain physical insight into the super absorption of the emitted power, we decompose the emitted power spectrum due to TE and TM polarized-field spatial harmonics and analyze their interaction with the HM. We use the equivalent transmission line theory provided in chapters 2, 3, and 5 in Ref. 1. The total power $P_{\mathrm{tot}} = P_{\mathrm{u}} + P_{\mathrm{d}}$ coupled to TE and TM waves (where u and d subscripts denote upward and downward directions, respectively) is computed by spectral integrals as

$$P_{\mathrm{u,d}} = \frac{\omega^2 |p_x|^2}{8\pi} \int_0^{+\infty} p_{\mathrm{u,d}}(k_t) dk_t, \tag{4}$$

where

$$p_{\mathrm{u,d}}(k_t) = \frac{\mathrm{Re}\left[Y_{\mathrm{u,d}}^{\mathrm{TM}*}(k_t)\right]}{\left|Y_{\mathrm{tot}}^{\mathrm{TM}}(k_t)\right|^2} k_t + \frac{\mathrm{Re}\left[Y_{\mathrm{u,d}}^{\mathrm{TE}*}(k_t)\right]}{\left|Y_{\mathrm{tot}}^{\mathrm{TE}}(k_t)\right|^2} k_t \tag{5}$$

are the upward and downward directed power spectra, respectively, where "$*$" indicates complex conjugate operation. The terms $Y_{\mathrm{u,d}}^{\mathrm{TM,TE}}$ represent equivalent spectral admittances at the dipole location, looking upward ($+z$ direction) or downward ($-z$ direction), for TE and TM waves. Following Ref. 1, where their expressions and physical interpretation are provided, we recall that the wave admittances relative to the upper half-space are simply given by

$$Y_{\mathrm{u}}^{\mathrm{TM}} = \frac{\omega \varepsilon_{\mathrm{u}} \varepsilon_0}{k_{z,\mathrm{u}}}, \quad Y_{\mathrm{u}}^{\mathrm{TE}} = \frac{k_{z,\mathrm{u}}}{\omega \mu_0}, \tag{6}$$

where $k_{z,\mathrm{u}} = \sqrt{\varepsilon_{\mathrm{u}} k_0^2 - k_t^2}$. The downward admittances $Y_{\mathrm{d}}^{\mathrm{TM}}$ and $Y_{\mathrm{d}}^{\mathrm{TE}}$ in Eq. (5) (evaluated at the dipole location) in the case of a homogeneous HM half-space have to be calculated using transfer matrix method[19] and the TM and TE wave admittances

$$Y^{\mathrm{TM}} = \frac{\omega \varepsilon_t \varepsilon_0}{k_{z,\mathrm{d}}^{\mathrm{TM}}}, \quad Y^{\mathrm{TE}} = \frac{k_{z,\mathrm{d}}^{\mathrm{TE}}}{\omega \mu_0}, \tag{7}$$

where $k_{z,\mathrm{d}}^{\mathrm{TE,TM}}$ is calculated using either the TE or TM dispersion relation in Eq. (3). In the case of multilayered HM, instead, the downward admittances $Y_{\mathrm{d}}^{\mathrm{TM}}$ and $Y_{\mathrm{d}}^{\mathrm{TE}}$ in Eq. (5) are calculated applying Bloch theorem to the multilayered structure and transfer matrix method.[19] Following Ref. 1, the total admittance in Eq. (5) is defined as

$$Y_{\mathrm{tot}}^{\mathrm{TM,TE}}(k_t) = Y_{\mathrm{d}}^{\mathrm{TM,TE}}(k_t) + Y_{\mathrm{u}}^{\mathrm{TM,TE}}(k_t). \tag{8}$$

Analogous calculations can be performed also for the power emitted by a z-directed dipole p_z, which is not reported here for brevity. Note that with these expressions one can calculate the spectral power content of TE/TM waves, independently, and to the authors' knowledge, this exact spectral analysis has not been previously investigated for composite HMs. Moreover, this formalism can also model the effect induced by the periodic nature of the HM via Bloch theory,[19] as was explained in regard to Fig. 3. The ratio $P_{\mathrm{tot}}/P_{\mathrm{free\ space}}$ of the total power emitted by an elementary dipole located at a distance $h = 15$ nm from the interface between free space ($\varepsilon_{\mathrm{u}} = 1$) and five different kinds of bottom media, namely, bulk silica, bulk silver, HMm (HM with metal as the topmost layer), HMd (HM with dielectric as the topmost layer), and HM EMA (HM modeled by EMA), is plotted versus frequency in Fig. 4(a). $P_{\mathrm{free\ space}}$ is the total power emitted by the same dipole in free space. Similarly, in Fig. 4(b), the ratio $P_{\mathrm{tot}}/P_{\mathrm{free\ space}}$ is plotted versus the dipole distance h from the interface, at 400 THz. In the HM cases, we assume the period equal to $d = d_1 + d_2 = 10$ nm, as in Fig. 3.

Looking at the ratio $P_{\mathrm{tot}}/P_{\mathrm{free\ space}}$ in Fig. 4, without considering the HM EMA result for the moment, the highest emitted power occurs for the HMm case (slightly larger than the HMd case), and the smallest for the bulk silver case, over a wide frequency band. We note, however, that HM EMA overestimates scattered power amounts for low frequencies or low distances h, and the explanation behind this fact will be provided in the discussion regarding Fig. 5. The power emitted by an elementary dipole at a distance $h = 15$ nm is about 7 to 15 times higher than the power emitted by the same dipole in free space in the case of HM bottom half-space [Fig. 4(a)]. Moreover, for the HM case, the ratio $P_{\mathrm{tot}}/P_{\mathrm{free\ space}}$ increases almost exponentially if h is decreased, as shown in Fig. 4(b), thanks to the coupling of power between evanescent spectrum in free space and propagating spectrum in the HM. This clearly indicates that a large boost of emitted power occurs when the dipole is very close to the HM.

To investigate the physical mechanism causing the enhancement of the power emission by a dipole in proximity of a HM, and the suitability to super absorption capabilities, we report in Fig. 5 the downward and upward spectra p_{d} and p_{u} in Eq. (5) normalized by k_0. The very wide spectrum of $p_{\mathrm{d}}(k_t)$ coupled to the HM, from $k_t \approx 2.1k_0$ to $k_t \approx 14.3k_0$,

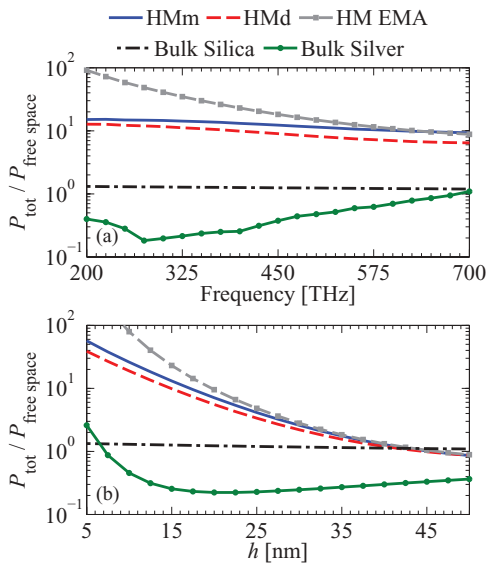

FIG. 4. (Color online) The ratio $P_{tot}/P_{free\ space}$ related to an elementary transverse dipole located near the interface between free space and five kinds of media: bulk silica, bulk silver, HMm (HM with metal as the topmost layer), HMd (HM with dielectric as the topmost layer), and HM EMA (HM modeled by EMA). The multilayered HM is composed of 5-nm-thick silver and silica layers. (a) The dipole is located at a distance $h = 15$ nm, and frequency is varied. (b) The dipole location h is varied at 400 THz.

is clearly seen in Fig. 5(a), in agreement with the dispersion diagram plotted in Fig. 3, which shows the k_t spectrum where TM waves have relatively small α_z and thus are mainly propagating. The upward power spectrum is instead present only for $k_t < k_0$, the propagating spectrum in free space. Also note that EMA results in a wider propagating spectrum

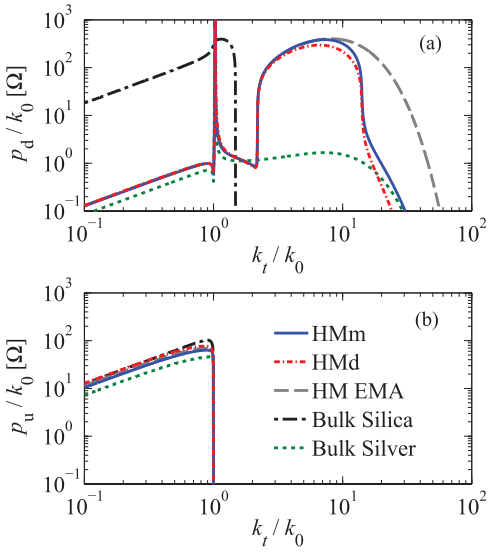

FIG. 5. (Color online) (a) Downward, p_d, and (b) upward, p_u, spectral power emitted by a transverse dipole located at $h = 15$ nm at 400 THz, for the same case considered in Fig. 4. Note the large power spectrum p_d for k_t/k_0 between 2.1 and 14.3 for the bottom HMm and HMd cases, and between 2.1 and 36.5 for the bottom HM EMA case.

inside the HM, from $k_t \approx 2.1k_0$ to $k_t \approx 36.5k_0$, eventually in disagreement with Bloch theorem for large k_t spectrum, specifically in the region $14.3k_0 < k_t < 36.5k_0$. As mentioned in Sec. II, EMA predicts that any $k_t > k_0\sqrt{\varepsilon_z}$ is allowed to propagate in the HM; however, due to the dipole distance from the HM interface, a large k_t spectrum cannot couple power into the HM because of the free space evanescent field decay proportional to $\exp(-\sqrt{k_t^2 - k_0^2}h)$. It is this evanescent decay that leads to power spectrum $p(k_t)$ decay after $k_t \approx 36.5k_0$ in the HM EMA case in Fig. 5(a). This fact implies that the closer is the distance h of the dipole from the HM, the larger is the power coupled into the HM.

Observing the power spectrum in Fig. 5, it is also useful to explain why the total scattered power evaluated with EMA as in Fig. 4(a) is overestimated when compared to the one calculated with Bloch theory, in the low-frequency region. The power spectrum difference between EMA and Bloch theory is mainly in the interval $k_{t,\max}^{\text{Bloch}} < k_t < k_{t,\max}^{\text{EMA}}$, where $k_{t,\max}^{\text{Bloch}}$ and $k_{t,\max}^{\text{EMA}}$ are evaluated as follows. The largest spectral component k_t of the field emitted by the source and coupled to the HM under EMA is determined assuming that the power spectrum decays as $\exp(-\sqrt{k_t^2 - k_0^2}h)$, and it is considered negligible when $\sqrt{k_t^2 - k_0^2}h > \xi$, where $\xi \geqslant 1$ is a predetermined number. This shows that the upper boundary of the k_t spectrum coupled to the HM under EMA (i.e., $k_t < k_{t,\max}^{\text{EMA}}$) is $k_{t,\max}^{\text{EMA}} = \sqrt{k_0^2 + (\xi/h)^2} \approx \xi/h$. Note that this upper limit is independent of frequency in the assumption $\xi^2/h^2 \gg k_0^2$ (fully verified in our case).

The upper spectral limit $k_{t,\max}^{\text{Bloch}}$ denotes the maximum spectrum able to propagate in the HM using the more precise Bloch theory, and it is determined by β_z approaching the Brillouin zone edge. By looking at the dispersion diagrams in Fig. 6 relative to different frequencies, one can observe that

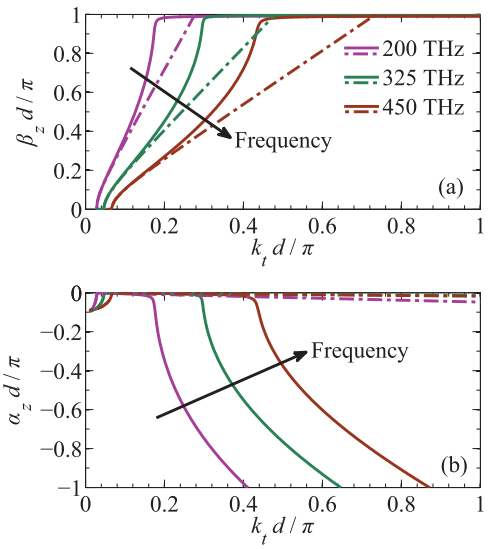

FIG. 6. (Color online) $k_z - k_t$ dispersion diagram normalized by π/d, at the three frequencies shown in the legend, obtained via Bloch theory (solid) and EMA (dashed dotted). (a) Real and (b) imaginary parts of the wave number $k_z = \beta_z + i\alpha_z$ in the multilayered HM considered in Fig. 4.

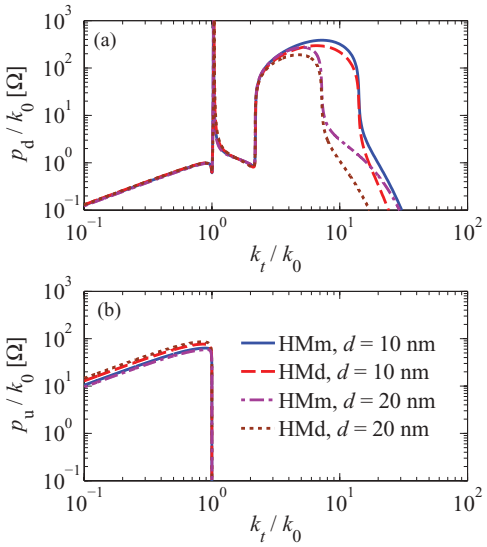

FIG. 7. (Color online) (a) Downward, p_d, and (b) upward, p_u, spectral power emitted by a transverse dipole located at $h = 15$ nm at 400 THz, for the same case considered in Fig. 4, considering the two periods in the legend (individual silver and silica layers are assumed with equal thicknesses).

the $k_{t,\max}^{\text{Bloch}}$ decreases for decreasing frequency. However, since the ratio $k_{t,\max}^{\text{Bloch}}/k_0$ remains almost constant and equal to about 14, as in Sec. II for the multilayered HM under analysis, we can say that $k_{t,\max}^{\text{Bloch}} \approx Kk_0$, where K is a proportionality constant determined mainly by the periodicity of the multilayered HM (see the discussion regarding Fig. 7). This means that the difference between power spectra able to couple power into the HM under EMA and Bloch theory is as wide as $\Delta k_t = k_{t,\max}^{\text{EMA}} - k_{t,\max}^{\text{Bloch}} \approx \xi/h - Kk_0$. We note that Δk_t increases for decreasing frequency, hence leading to higher disagreement between EMA and Bloch theory at lower frequencies, and explaining the power overestimation by EMA in Fig. 4(a) in the low-frequency region of the plot.

In Fig. 7, we analyze the power spectra of the HM for two illustrative cases: the one shown in Fig. 5 with a metamaterial period $d = d_1 + d_2 = 10$ nm, and another one with doubled period $d = d_1 + d_2 = 20$ nm (still keeping the same d_1/d_2 of the case in Fig. 5). This analysis is performed to stress that the metamaterial physical parameters impact the propagating spectrum inside the HM, which tends to be narrower as the period of the HM is increased. The upper edge of the propagating spectrum inside the HM shifts from $k_t \approx 14.3k_0$ (10 nm period) to $k_t \approx 7.1k_0$(20 nm), showing that the period of the HM needs to be minimized in order to have a wide propagating spectrum inside the HM that can be employed to couple power coming from the evanescent spectrum in free space.

IV. POWER SCATTERED BY A NANOPARTICLE CLOSE TO A HYPERBOLIC METAMATERIAL

We show and explain now the phenomenon of strong absorption by the HM when a passive nanoscatterer in proximity of the HM interface is illuminated. Inspired by the experimental results in Ref. 22, we focus on understanding how a nanosphere's scattered power is affected by its size and material properties. Hence, consider a silver nanosphere located as in Fig. 1(b), excited by a linearly polarized (say along the x direction) plane wave with normal incidence. The nanosphere is modeled as an equivalent electric dipole via the single dipole approximation,[23,24] and its induced dipole moment located at the center of the nanosphere (thus at a distance from the HM equal to the radius r) is given by $p_x = \alpha_{xx} E_x^{\text{loc}}$, where α_{xx} is the electric polarizability (Clausius–Mossotti expression reported in Refs. 23 and 24), and E_x^{loc} is the local electric field acting on the nanosphere. In particular,

$$E_x^{\text{loc}} = E_x^{\text{pw}} + E_x^s, \tag{9}$$

where E_x^{pw} is the total plane wave field, sum of the incident plane wave and the one reflected at the HM interface, evaluated at the nanosphere's center. Furthermore, $E_x^s = G_{xx}^s p_x$ represents the field produced by the dipole itself, and evaluated at its location, which accounts for the scattering by the bottom half-space. Accordingly, the term G_{xx}^s is the $\hat{\mathbf{x}}\hat{\mathbf{x}}$ component of the regularized dyadic Green's function, i.e., it does not account for the free-dipole field but includes all the spectral terms reflected by the HM interface. Accordingly, it is given by the spectral representation

$$G_{xx}^s = \frac{i\omega}{4\pi} \int_0^{+\infty} \left[\frac{\Gamma_{\text{d}}^{\text{TM}}(k_t)}{2Y_{\text{u}}^{\text{TM}}(k_t)} + \frac{\Gamma_{\text{d}}^{\text{TE}}(k_t)}{2Y_{\text{u}}^{\text{TE}}(k_t)} \right] k_t dk_t, \tag{10}$$

where

$$\Gamma_{\text{d}}^{\text{TM,TE}}(k_t) = \frac{Y_{\text{u}}^{\text{TM,TE}}(k_t) - Y_{\text{d}}^{\text{TM,TE}}(k_t)}{Y_{\text{u}}^{\text{TM,TE}}(k_t) + Y_{\text{d}}^{\text{TM,TE}}(k_t)} \tag{11}$$

are the plane-wave reflection coefficients[1] of TE and TM spectral components with transverse wave number k_t, looking towards the $-z$ direction, and evaluated at the nanosphere center location. By solving for the scatterer's dipole moment, one obtains the closed form expression

$$p_x = \frac{\alpha_{xx}}{1 - \alpha_{xx} G_{xx}^s} E_x^{\text{pw}}. \tag{12}$$

The total plane field at the nanosphere's center is given by $E_x^{\text{pw}} = E_x^{\text{inc}}[1 + \Gamma_{\text{d}}(0)]$, where E_x^{inc} is the incoming normally incident plane wave, and $\Gamma_{\text{d}}(0)$ is its reflection coefficient evaluated at the nanosphere's center. This method is accurate when the nanosphere is subwavelength and not far from its first Fröhlich resonance,[23] so that the electric dipolar term is dominant compared with the field due to higher multipolar terms. Once the dipole moment p_x of the nanosphere is determined, its scattered power toward the upper (free space, P_{u}^s) and lower (P_{d}^s) spaces is evaluated by using Eq. (4). The advantage of this semi-analytical method is that it breaks down each scattering process into its basic components and provides a clear physical insight.

The total scattered power $P_{\text{tot}}^s = P_{\text{u}}^s + P_{\text{d}}^s$ due to a silver nanosphere located on top of six possible substrates (HMd, HMm, HM EMA, bulk silver, bulk silica, and free space) under linearly polarized, normally incident plane wave E_x^{inc} (with 1 V/m electric field amplitude) is shown in Fig. 8(a) for a nanosphere with radius $r = 15$ nm versus frequency, and in Fig. 8(b) versus the nanosphere's radius r at 400 THz. The passive silver nanosphere on top of HMd and HMm apparently scatters one or two orders of magnitude more total power than

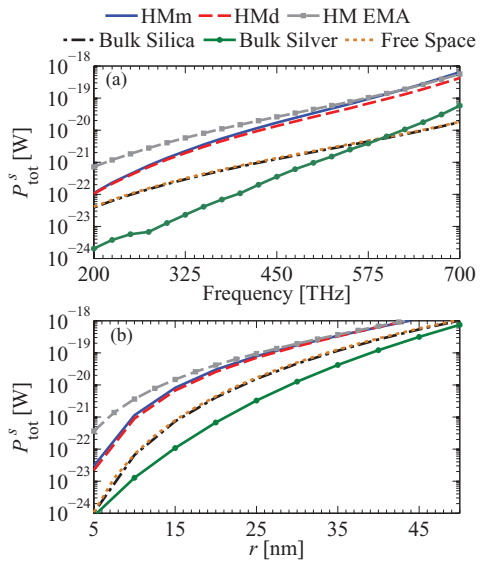

FIG. 8. (Color online) Total power P^s_{tot} scattered by a silver nanosphere located on the surface of six kinds of media: bulk silver, bulk silica ($\varepsilon_{SiO_2} = 2.2$), free space, HMm, HMd, and HM EMA composed of silver and silica layers of thickness 5 nm, under plane wave incidence ($|E^{inc}_x| = 1$ V/m) when (a) $r = 15$ nm and frequency is varied and (b) at 400 THz varying the nanosphere radius r.

when on top of bulk silica, free space, or bulk silver, between 200 and 700 THz [in agreement with the total power emitted by an elementary transverse dipole shown in Fig. 4(a)]. Note also that HM EMA gives overestimated scattered power amounts for smaller frequency/radius ranges in agreement with the discussion in Sec. III. The difference in scattered power among all substrate cases is less evident when the nanosphere radius is increased, as shown in Fig. 8(b), though the total power scattered by the nanosphere in the case of the HM substrates is still significantly larger than in the other bulk substrate cases. In Fig. 9, the ratio P^s_d/P^s_u is plotted (a) for a nanosphere with $r = 15$ nm versus frequency, and (b) at 400 THz versus the nanosphere radius r. One shall notice a remarkable effect—that the scattered power into the bottom space P^s_d is much larger than the power scattered into the upper space ($P^s_d \gg P^s_u$) for HMm and HMd (where HMm has a larger ratio), indicating that the nanosphere's scattered field is mainly absorbed by the HM (and giving direct proof of super absorption capabilities). Note that HM EMA gives overestimated results for smaller frequencies or radii, as explained in Sec. III. The case with bulk silver bottom space yields the lowest P^s_d/P^s_u ratio in most of the shown frequency band when compared with all other substrates except free space, where power is evenly scattered and thus $P^s_d/P^s_u = 1$. When the radius of the metal nanosphere is decreased, the ratio P^s_d/P^s_u increases for cases with HMd, HMm, HM EMA, and bulk silver bottom spaces because the power coupled to these media is related to a wide k_t spectrum that is purely evanescent in free space (where HM hosts mainly propagating waves, and bulk silver hosts mainly evanescent waves related to losses), whereas the case with bulk silica bottom space is slightly affected. For small nanospheres, e.g., $r = 15$ nm or smaller, the downward power exceeds the upward power by at least two orders of magnitude. Therefore, we can observe that a proper distance and size shall be selected for the nanosphere to enhance its scattered power, and direct it toward the HM: If the nanosphere is much smaller than the wavelength, it will not scatter light efficiently; whereas if it is too large, it does not couple efficiently to the HM's high density of states, and the scattering directed toward the HM is weak (i.e., less power will be coupled into the HM). For the sake of completeness, we show in Fig. 10 the power scattered by the nanosphere into the upper space for the cases reported in Fig. 8 and Fig. 9. When looking at Fig. 10(a), we note that in the HM cases, the nanosphere scatters less power (up to two orders of magnitude) into the upper space until 450 THz. For the remaining frequency range, as well as for the result in Fig. 10(b), the power scattered in the upper half-space in the presence of the HM is comparable to the one scattered when

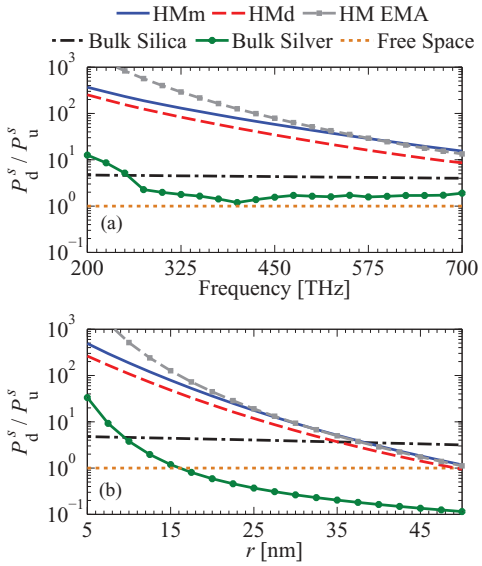

FIG. 9. (Color online) Ratio of downward over upward power P^s_d/P^s_u, for the same case considered in Fig. 8.

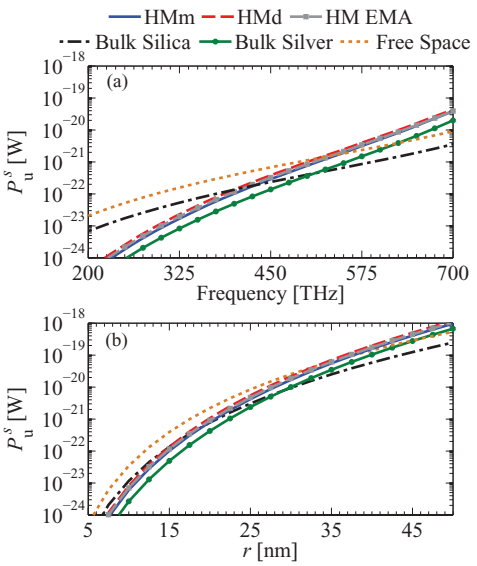

FIG. 10. (Color online) The upward scattered power P^s_u for the same case considered in Fig. 8.

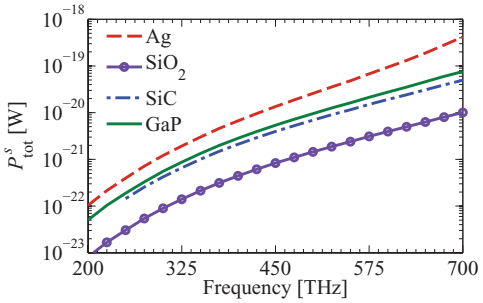

FIG. 11. (Color online) Total power $P^s_{\rm tot}$ scattered by silver (Ag), silica (SiO_2), silicon carbide (SiC), and gallium phosphide (GaP) nanospheres ($r = 15$ nm) located on top of the HMd in Fig. 8 composed of silver and silica layers of thickness 5 nm, varying frequency under plane wave incidence ($|E^{\rm inc}_x| = 1$ V/m).

the nanosphere is in free space. Moreover, the amount of the scattered power into the upper space increases as the radius is increased. We however know from Fig. 8 that the total scattered power is about 1 to 2 orders of magnitude larger than the one in free space. This is a promising quality of the metamaterial under study: Not only is the downward power scattered by the nanosphere on top of HM increased (dictating suitability to absorption capabilities), but also the upward scattered power is reduced or comparable to the one scattered in free space over a wide frequency band.

Lastly, we inspect the influence of the nanosphere's material on the scattered power. We consider the HMd substrate in Fig. 8 and nanospheres with radius $r = 15$ nm made of four materials, namely, silver (Ag, with negative and large permittivity[17]), silica (SiO_2 with small and positive permittivity $\varepsilon_{SiO_2} = 2.2$), silicon carbide (SiC, positive and moderate permittivity[25]), and gallium phosphide (GaP, large positive permittivity with losses[25,26]), and we show their scattered total power in Fig. 11. Apparently, when the permittivity of the nanosphere's material increases in absolute value (Ag, GaP), the total power scattered by the nanosphere increases as well. Although the $P^s_{\rm d}/P^s_{\rm u}$ ratio does not depend on the excitation of the dipole itself, the material of the scatterer effectively determines how much power of the incident plane wave is scattered. Further conclusions about the usage of sets of scatterers on top of HM for achieving low reflectance need modeling of distributed scatterers on a HM surface and will be the object of future work.

V. CONCLUSION

We have shown via spectral theory that: (i) the power scattered by a passive nanosphere located in the proximity of a HM is increased; and (ii) scatterers located on top of HMs scatter almost all power toward the HM. Both HM EMA and multilayer implementations (HMm, HMd) lead to similar super absorption properties (in some frequency ranges, EMA overestimates absorption). Therefore, HMs have a clear potential of enhancing the decay rate of emitters near its surface and also for designing efficient and innovative absorbers. A list of foreseen applications of this "super absorber" with unprecedented performance in terms of bandwidth and wide angle of operations includes radar cross section reduction, near-field absorbers, improved solar spectrum absorption, and infrared absorbers.

*Corresponding author: f.capolino@uci.edu (http://capolino.eng.uci.edu)

[1]L. B. Felsen and N. Marcuvitz, *Radiation and Scattering of Waves* (Prentice-Hall, Upper Saddle River, NJ, 1973).
[2]D. R. Smith and D. Schurig, Phys. Rev. Lett. **90**, 077405 (2003).
[3]G. V. Naik, J. Liu, A. V. Kildishev, V. M. Shalaev, and A. Boltasseva, Proc. Nat. Acad. Sci. **109**, 8834 (2012).
[4]J. B. Pendry and S. A. Ramakrishna, Physica B Condens. Matter **338**, 329 (2003).
[5]K. J. Webb and M. Yang, Opt. Lett. **31**, 2130 (2006).
[6]X. Li and F. Zhuang, J. Opt. Soc. Am. A **26**, 2521 (2009).
[7]Y. Jin, Prog. Electromag. Res. PIER **105**, 347 (2010).
[8]C. Della Giovampaola, M. Albani, and F. Capolino, in *Metamaterials Congress* (Barcelona, Spain, 2011).
[9]R. Kotyński, T. Stefaniuk, and A. Pastuszczak, Appl. Phys. A **103**, 905 (2011).
[10]Z. Liu, Z. Liang, X. Jiang, X. Hu, X. Li, and J. Zi, Appl. Phys. Lett. **96**, 113507 (2010).
[11]X. Ni, G. Naik, A. Kildishev, Y. Barnakov, A. Boltasseva, and V. Shalaev, Appl. Phys. B **103**, 553 (2011).
[12]H. N. S. Krishnamoorthy, Z. Jacob, E. Narimanov, I. Kretzschmar, and V. M. Menon, Science **336**, 205 (2012).
[13]T. U. Tumkur, L. Gu, J. K. Kitur, E. E. Narimanov, and M. A. Noginov, Appl. Phys. Lett. **100**, 161103 (2012).
[14]E. E. Narimanov, H. Li, Y. A. Barnakov, T. U. Tumkur, and M. A. Noginov, arXiv:1109.5469.
[15]P. A. Belov and Y. Hao, Phys. Rev. B **73**, 113110 (2006).
[16]L. D. Landau, E. M. Lifshitz, and L. P. Ptaevskii, *Electrodynamics of Continuous Media*, 2nd ed. (Butterworth-Heinemann, Oxford, UK, 1984), p. 339.
[17]P. B. Johnson and R. W. Christy, Phys. Rev. B **6**, 4370 (1972).
[18]O. Kidwai, S. V. Zhukovsky, and J. E. Sipe, Opt. Lett. **36**, 2530 (2011).
[19]D. M. Pozar, *Microwave Engineering*, 3rd ed. (Wiley, Hoboken, NJ, 2005).
[20]S. Campione, S. Steshenko, M. Albani, and F. Capolino, Opt. Express **19**, 26027 (2011).
[21]S. Campione, S. Steshenko, and F. Capolino, Opt. Express **19**, 18345 (2011).
[22]T. U. Tumkur, J. K. Kitur, B. Chu, L. Gu, V. A. Podolskiy, E. E. Narimanov, and M. A. Noginov, Appl. Phys. Lett. **101**, 091105 (2012).
[23]C. F. Bohren and D. R. Huffman, *Absorption and Scattering of Light by Small Particles* (Wiley, New York, 1983).
[24]S. Steshenko and F. Capolino, in *Theory and Phenomena of Metamaterials*, edited by F. Capolino (CRC Press, Boca Raton, FL, 2009).
[25]E. Palik, *Handbook of Optical Constants of Solids* (Academic Press, New York, 1985).
[26]D. E. Aspnes and A. A. Studna, Phys. Rev. B **27**, 985 (1983).